



**Showcasing research from Professor Suzana Nunes Laboratory (Nanostructured Polymeric Membranes Laboratory), Advanced Membranes and Porous Materials Center, King Abdullah University of Science and Technology, Thuwal, Saudi Arabia.**

**Bio-based solvents for polyolefin dissolution and membrane fabrication: from plastic waste to value-added materials**

The use of two bio-based renewable solvents,  $\alpha$ -pinene, and  $\alpha$ -limonene, was demonstrated for polyolefins dissolution. Membranes from polypropylene as commercial pellets or from food packaging waste were prepared by dissolving it in  $\alpha$ -pinene, followed by thermally induced phase separation. Optimized membranes exhibited efficient water-in-toluene emulsion separation performance with approximately 95% water rejection and 99.97% toluene purity.

**As featured in:**


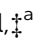




See Suzana P. Nunes *et al.*,  
*Green Chem.*, 2023, **25**, 966.



Cite this: *Green Chem.*, 2023, **25**, 966

# Bio-based solvents for polyolefin dissolution and membrane fabrication: from plastic waste to value-added materials†

Malinalli Ramírez-Martínez, <sup>‡a,b</sup> Sandra L. Aristizábal, <sup>‡a,b</sup> Gyorgy Szekely <sup>a,b,c</sup> and Suzana P. Nunes <sup>\*a,b,d</sup>

Membrane technology is a low-footprint and highly efficient industrial separation process. While more stable membranes could substantially contribute to modernizing the chemical industry, sustainability must be seen holistically. Polymer sources, solvents, and recycling strategies that adhere to the strategic concepts of the circular economy should be considered at the membrane design stage. Recycling plastic waste into separation membranes can help remediate the environmental impact of the current plastic pollution. Polyolefins are the most manufactured and used polymer family, and their high chemical resistance and low price are attractive for membrane preparation. However, their limited solubility in mainly non-renewable solvents at high temperatures restricts their processability and recycling. In this work, we present the use of polypropylene (PP) and low-density polyethylene (LDPE) as the source of membrane preparation by their dissolution in two bio-based and renewable solvents ( $\alpha$ -pinene and D-limonene). The thermal properties and phase separation behavior were studied and phase diagrams were obtained. Liquid–liquid phase separation and spherulitic morphology were observed for the three studied systems. PP membranes were obtained by a thermally induced phase separation (TIPS) process employing  $\alpha$ -pinene as a solvent, and food packaging plastic waste or commercially available PP pellets in the polymer dope solution. The obtained membranes were tested for water-in-oil emulsion separations. The influence of the polymer content and the quenching media on the morphology, mechanical and thermal properties, and water contact angle was investigated. PP membranes were fabricated with 20–30 wt% polymer contents using water at 4 °C and 20 °C as quenching media. The contact angles were higher than 150° under oil enabled efficient water-in-toluene emulsion separation, where approx. 95% water rejection and an average of 99.97% toluene purity were achieved.

Received 24th August 2022,  
Accepted 24th November 2022

DOI: 10.1039/d2gc03181g

rsc.li/greenchem

## 1. Introduction

Membrane technology plays an essential role in sustainable industrial practices due to its low environmental footprint during operation compared to conventional thermal separation methods.<sup>1,2</sup> In addition, membranes exhibit remarkable

performance in applications such as air and water purification, biomedical devices, energy production, food processing, chemical separations, and others.<sup>2–5</sup> However, when focusing on the membrane fabrication stage, the overall membrane's sustainability can be further improved.<sup>6–9</sup>

Polymeric membranes lead the market over ceramic ones due to their low cost, processability, scalability, and versatility.<sup>4</sup> They are mainly prepared by phase separation processes triggered by changes in the thermodynamic conditions. A homogeneous polymer casting solution separates into a polymer-lean phase (incipient pores) and a polymer-rich phase, following a spinodal decomposition or a nucleation and growth mechanism. The polymer-rich phase gels and solidifies, kinetically trapping the porous structure.<sup>10,11</sup> Three of the most applied techniques are thermally induced phase separation (TIPS), non-solvent induced phase separation (NIPS), and vapor induced phase separation (VIPS), in which the phase separation is triggered by a change in temperature, solvent and non-solvent exchange in the liquid state, and exposure to a

<sup>a</sup>Environmental Science and Engineering Program, Biological and Environmental Science and Engineering Division (BESE), King Abdullah University of Science and Technology (KAUST), 23955-6900 Thuwal, Saudi Arabia.

E-mail: [suzana.nunes@kaust.edu.sa](mailto:suzana.nunes@kaust.edu.sa); Tel: +966128082771

<sup>b</sup>Advanced Membranes and Porous Materials (AMPM) Center, King Abdullah University of Science and Technology (KAUST), 23955-6900 Thuwal, Saudi Arabia

<sup>c</sup>Chemical Science Program, King Abdullah University of Science and Technology (KAUST), 23955-6900 Thuwal, Saudi Arabia

<sup>d</sup>Chemistry Program, King Abdullah University of Science and Technology (KAUST), 23955-6900 Thuwal, Saudi Arabia

†Electronic supplementary information (ESI) available. See DOI: <https://doi.org/10.1039/d2gc03181g>

\*These authors contributed equally to this work.





non-solvent in the gas state, respectively.<sup>12,13</sup> To date, the membrane fabrication industry uses mainly non-renewable and toxic solvents, such as *N*-methylpyrrolidone (NMP), *N,N*-dimethylacetamide (DMAc), and *N,N*-dimethylformamide (DMF), and fossil-based polymers.<sup>14–16</sup> Such solvents and polymers have been estimated to contribute to global warming, human health threats, and fossil resource scarcity.<sup>8</sup> In response, strategies following the principles of circular economy and green chemistry are being increasingly studied over the last few years for their implementation in membrane fabrication processes. Two examples are the utilization of greener solvents and alternative polymer sources.<sup>6,7,16–19</sup>

Greener solvents in membrane preparation such as methyl lactate, ethyl lactate, Cyrene<sup>TM</sup>, PolarClean®, natural organic carbonates, ionic liquids, vegetable oil, and others, have shown good compatibility with different polymers.<sup>15,20–27</sup> For example, Rasool *et al.*<sup>21</sup> fabricated asymmetric cellulose acetate (CA) nanofiltration membranes *via* NIPS using bio-derived methyl lactate and 2-methyl tetrahydrofuran as a solvent and co-solvent, respectively. The optimized membranes showed a Rose Bengal (1018 g mol<sup>−1</sup>) rejection above 99% in water, making them promising candidates for applications in the nanofiltration range. Wang *et al.*<sup>15</sup> used the synthetic non-toxic PolarClean® for CA dissolution to fabricate nanofiltration membranes and to dissolve polysulfone (PSF) and polyether-sulfone (PES) for preparing ultrafiltration membranes *via* the NIPS process. Marino *et al.*<sup>20</sup> reported the use of Cyrene<sup>TM</sup>, a bio-solvent derived from nonfood cellulosic sources, for PES and poly(vinylidene fluoride) (PVDF) membrane preparation by NIPS obtaining pore sizes around 500 nm and pure water permeance around 550 L m<sup>−2</sup> h<sup>−1</sup> bar<sup>−1</sup>. Ismail *et al.*<sup>28</sup> reported the fabrication of PVDF membranes employing ethylene carbonate (EC) as a solvent during a combined NIPS and TIPS process, which exhibited an outstanding performance for water desalination by membrane distillation, with more than 99.97% salt rejection factor. These encouraging works serve as an example of the high potential of green solvents for replacing traditional non-renewable ones while maintaining a competitive performance to be applied in diverse applications. Nevertheless, the use of green solvents for the dissolution of chemically stable polymers is still challenging. This is the case for polyolefins such as polyethylene (PE) and polypropylene (PP), commonly dissolved in fossil-derived hydrocarbons (*e.g.* *p*-xylene, dodecane, decalin, and paraffin oils) at temperatures ranging from 140 to 250 °C. Beside their processing limitations, PP and PE significantly contribute to plastic pollution, considering that they account for nearly half of the plastics produced worldwide for their use in applications such as food packaging, bottle containers, automotive parts, toys, and houseware products (182 million metric tons produced in 2021)<sup>29,30</sup> and that only around 8.8% of the plastics are recycled.<sup>31,32</sup> A 2017 report by the Ellen Macarthur Foundation estimated that plastic packaging materials are devalued by 95% after one short use, which translates to economic losses of USD 80–120 billion annually.<sup>33</sup> Thus, efforts to directly transform plastic waste into value-added products, such as polymeric membranes, is a step

forward toward more sustainable industrial practices, specifically in the membrane industry.<sup>6,34,35</sup>

Several works have reported the successful utilization of plastic waste for membrane fabrication. Pulido *et al.*<sup>36</sup> fabricated polyethylene terephthalate (PET) ultrafiltration membranes from plastic waste by NIPS, showing good performance even at temperatures up to 100 °C and high resistance towards harsh solvents. Lai *et al.*<sup>37</sup> reported the use of polystyrene (PS) waste as a material source for fabricating waterproof CO<sub>2</sub> separation membranes through hot-pressing. Keles and Uysal<sup>38</sup> optimized the fabrication of low-density polyethylene (LDPE) and acrylic fiber membranes by electrospinning using shrink film packaging waste as the polymer source for wastewater treatment applications. These examples demonstrate the technical viability of using plastic waste as feedstock for membrane fabrication and the potential for environmental remediation.

In this work, we contribute to sustainability in polyolefin membrane fabrication through two approaches. First, by utilizing renewable bio-based solvents for PP and LDPE dissolution, and second, by implementing the direct recycling of plastic waste as a polymer source in the membrane fabrication process. The selected bio-based solvents were  $\alpha$ -pinene and  $\beta$ -limonene, belonging to the terpene family, the largest class of natural products (produced by all plants), and have a long trajectory in human healthcare, with a FDA (U.S. Food and Drug Administration) approval for their use in food and cosmetics.<sup>39–42</sup> They have been proposed as sustainable alternatives to fossil-derived solvents such as *n*-hexane for the extraction of valuable compounds, such as carotenoids, oil from seeds and microalgae, lipids, and aromas.<sup>43–45</sup>  $\beta$ -Limonene is produced from citrus fruits peels, a feedstock widely available from the juice industry waste, while  $\alpha$ -pinene is derived from gum turpentine, an essential oil distilled from the pine gum harvested from living pine trees or obtained as a side product of the pulp mill industry (Fig. S1†).<sup>46,47</sup> Their similar Hansen Solubility Parameters (HSP), compared to the petroleum-based *p*-xylene used in polyolefin dissolution, offers a great potential for their use as alternative greener solvents in PP and LDPE dissolution (Table S2†). Despite being renewable and widely available, their feasibility for polyolefin dissolution and membrane fabrication has not been studied to date, to the best of our knowledge. Here we proposed the use of  $\alpha$ -pinene and  $\beta$ -limonene for polyolefin dissolution and membrane fabrication.

The phase diagrams were obtained from the solubility and phase separation mechanism of commercially available PP and LDPE in the bio-based solvents. Then, the effect of polymer content and quenching media on the PP membrane's morphology, mechanical and thermal properties, and water contact angle were addressed. The resulting membranes were tested in water-in-oil emulsion separation as an example of the application of hydrophobic PP membranes. Commercially available PP and plastic waste from PP food packages were utilized as the polymer source for membrane fabrication, and the changes in the membrane's properties and performance were investigated and compared.



This study broadens the alternatives for polyolefin (PP and LDPE) dissolution and membrane fabrication with renewable bio-based solvents while revalorizing plastic waste, which can be of benefit for the polymers and membrane fields in the transition to a circular economy following the green chemistry principles.

## 2. Materials and methods

### 2.1. Materials

Low-density polyethylene ( $0.925 \text{ g mL}^{-1}$ ) and isotactic polypropylene ( $0.9 \text{ g mL}^{-1}$ ,  $250\,000 \text{ g mol}^{-1}$ ) pellets were purchased from Sigma Aldrich. Polypropylene food containers were obtained from a local supermarket and used as the plastic waste source. (1S)-(-)- $\alpha$ -Pinene was purchased from Merck Germany and D-limonene from MP Biomedicals. Heptane was purchased from Fisher Scientific, and toluene and *n*-hexane from VWR chemicals. A Span 80 non-ionic surfactant was obtained from Fluka Analytical. All materials were used as received without further purification. PP food containers were rinsed with acetone and used without further purification.

### 2.2. Membrane preparation

Flat-sheet membranes were prepared *via* TIPS, as illustrated in Fig. 1. Commercially available PP pellets were used for the polymer dope solution at 15, 20, and 25 wt% content in  $\alpha$ -pinene. The solutions were stirred at  $130^\circ\text{C}$  for three hours in a silicon oil bath to ensure complete polymer dissolution. Then, the stirring was stopped for three hours for de-bubbling while maintaining the temperature at  $130^\circ\text{C}$ . The obtained solution was cast with a casting knife with a  $250 \mu\text{m}$  gap on a stainless-steel plate, which was at the same temperature as the dope solution. The ambient relative humidity and temperature were 70% and  $20^\circ\text{C}$ . The film was then cooled by keeping the plate in air, or immersing the plate in water at  $20^\circ\text{C}$  or  $4^\circ\text{C}$  for five minutes to induce the phase separation. After the membrane was formed, the remaining solvent was removed by

immersing the membrane in ethanol for 24 h with a change of ethanol 12 h after the initial immersion. Finally, the obtained membranes were dried at room temperature for at least 24 h before filtration tests. The same procedure was applied for membranes prepared using PP waste from food containers.

### 2.3. Polymer solubility and phase diagrams

The bio-based solvents used in this work were initially identified by screening solvents with Hansen Solubility Parameters (HSP) similar to those of the fossil-based *p*-xylene (traditional solvent for polyolefin dissolution), utilizing the HSPiP software (Table S3†). According to Hansen,<sup>48</sup> the affinity of solvent 1 and polymer 2 can be quantified by calculating the solubility parameter distance ( $R_a$ ) based on eqn (1):

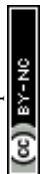
$$R_a^2 = 4(\delta_{d2} - \delta_{d1})^2 + (\delta_{p2} - \delta_{p1})^2 + (\delta_{hb2} - \delta_{hb1})^2 \quad (1)$$

where  $\delta_d$ ,  $\delta_p$ , and  $\delta_{hb}$  are the dispersion, polar, and hydrogen bonding solubility parameters, respectively. The distance  $R_a$  was calculated in comparison with PP and LDPE, and the position of the solvents in relation to the polymers was plotted in the HSP space considering an interaction radius of  $5 \text{ MPa}^{1/2}$  according to Van Krevelen and Te Nijenhuis<sup>49</sup> (Fig. S1†). The solubility of LDPE and PP in the selected solvent was evaluated by gradually adding commercially available polymer pellets to the solvent at a temperature of  $130^\circ\text{C}$ , and the dissolution limit was set to the concentration beyond which turbidity was observed in the system.

The phase diagrams were obtained by two methods: (i) observations of the dope solutions with different polymer contents on a Leica DM4500 P optical microscope and (ii) DSC measurements on a DSC 250 – TA instruments. The solutions were prepared in the same way for both methods. For optical microscopy observations, a drop of the polyolefin dope solution at  $130^\circ\text{C}$  was placed between two glass slips with a  $0.1 \text{ mm}$  thickness at the same temperature and rapidly transferred into a Linkam Hot Stage, pre-heated at  $140^\circ\text{C}$ . The temperature was maintained for five minutes and then decreased to room temperature ( $20^\circ\text{C}$ ) at a  $10^\circ\text{C min}^{-1}$  rate.



**Fig. 1** Schematic of polymeric membrane preparation *via* TIPS: preparation of the dope solution containing the polymer and the solvent, casting of the solution on a stainless steel plate, phase separation of the membrane by quenching media at a temperature below the crystallization temperature, and solvent extraction in ethanol.



The phase separation was observed during the cooling process under standard and polarized light. The cloud point (CP) was taken as the temperature at which the nucleus formation was observed with a 10× amplification lens.

DSC measurements were obtained by quenching the polyolefin dope solution with a specific composition in liquid nitrogen. A small piece of the solidified sample was then placed in a Tzero hermetic pan, heated to 140 °C and maintained for 20 min, cooled down to room temperature, kept for 10 min, and reheated to 140 °C to remove the thermal history of the polymer. Cooling–heating rates were 10 °C min<sup>−1</sup> in all cases, and the exothermic peak temperature was taken as the crystallization temperature ( $T_c$ ).

## 2.4. Characterization methods

The infrared spectra were obtained on a Nicolet iS10 instrument (Thermo Fisher Scientific) from 600 to 3800 cm<sup>−1</sup> with 32 scans. The molecular weight (MW) of the polymers was determined using an Agilent 1260 Infinity II High-Temperature Gel Permeation Chromatography (HT-GPC) Multi-Detector System equipment using 1,2,4-trichlorobenzene as a mobile phase.

Thermal analysis was performed on a TGA Q50 instrument under an air atmosphere at a heating rate of 20 °C min<sup>−1</sup> from 25 to 800 °C. DSC 250 and Tzero hermetic pans (TA instruments) were used for obtaining the crystallization and melting temperatures of polymers and PP membranes. In all cases, a heat–cool–heat cycle with an upper temperature of 230 °C was performed with a cooling–heating rate of 10 °C min<sup>−1</sup>.

SEM images were obtained on a Zeiss Merlin Electron Microscope. Samples for cross-section observations were prepared by breaking a piece of membrane in liquid nitrogen and placing it between two layers of conductive carbon tape. Silver paint was used on the borders of the membrane pieces to make contact between the carbon tape and the membrane. All samples were coated with a 3 nm iridium layer in a Quorum Q300RT sputter coater.

Water contact angles were measured on an FM40 Easy Drop instrument (KRÜSS). 2 µl water drop was utilized for air and under-oil measurements. All reported values are the average from three measurements.

Young's modulus, fracture strain, tensile strength, and toughness were obtained from strain *vs.* stress measurements on a Discovery DMA850 instrument. The stress ramp was set from 0.05 N to 18.00 N at a rate of 1.5 N min<sup>−1</sup>. Young's modulus was calculated as the slope of the linear section of the strain *vs.* stress curve; fracture strain was taken as the maximum strain value before the sample broke; tensile strength as the stress at which breaking occurred; and toughness was the area under the strain *vs.* stress curve. All reported values are the average from three measurements.

## 2.5. Membrane performance

**2.5.1. Pure hydrocarbon permeance.** Heptane, *n*-hexane, and toluene were used as model oils for testing pure hydrocarbon permeance. Tests were conducted using stainless steel

dead-end filtration cells with 400 mL total volume pressurized with five bar of nitrogen. For each test, 250 mL of the hydrocarbon were loaded into the cell, and the permeate weight was recorded during the experiment. Permeance ( $J$ ) for each membrane was calculated according to eqn (2):

$$J = \frac{V}{A \cdot t \cdot \Delta P} \quad (2)$$

where  $V$  is the permeated volume of hydrocarbon,  $A$  is the effective area of the membrane (3.46 cm<sup>2</sup>),  $t$  is time, and  $\Delta P$  is the pressure applied during filtration (five bar). Permeance was calculated with data from at least eight hours of flux in the steady state. The densities and viscosities of all hydrocarbons used in permeance tests are shown in Table S1.† The reported values are the averages from two membranes prepared independently under the same conditions.

**2.5.2. Water-in-toluene emulsion separation.** Water-in-toluene emulsions were prepared for testing the membrane's performance according to a procedure described elsewhere.<sup>50</sup> First, 114 mL of toluene and 0.5 g of Span 80 as a surfactant were stirred at 500 rpm for five minutes. Afterward, 1 mL of water was added. The mixture was stirred at 1000 rpm for six hours and then loaded into the filtration cell. Five bar was applied during the separation experiment, and the emulsion was maintained under stirring at 500 rpm to ensure emulsion homogeneity during the test. Water rejection, also denoted as separation efficiency ( $R$ ), was calculated from the water concentration in the permeate ( $C_p$ ) and in the feed ( $C_f$ ) expressed in ppm as shown in eqn (3):

$$R = \left(1 - \frac{C_p}{C_f}\right) \times 100\% \quad (3)$$

$C_p$  and  $C_f$  were measured two times in a Karl Fischer coulometric titrator (Mettler Toledo). Before each set of measurements, a 1000 ppm Hydranal water standard was measured, obtaining less than 1% error in all cases. Water drop size in the emulsions was determined by dynamic light scattering (DLS) in a Zetasizer Nano ZS (Malvern).

## 3. Results and discussion

Polyolefins are used on a large scale for disposable items and constitute an extensive part of plastic waste worldwide. Upcycling this plastic waste into useful materials, such as separation membranes, is a step forward toward more sustainable industrial practices. Nevertheless, the high chemical stability of polyolefins represents a challenge in terms of their processability since most membrane preparation methods are based on a solution process. Polyolefins are soluble only in a few selected solvents at high temperatures, where most of them are based on non-renewable sources. Green natural solvent alternatives have been seldomly identified (Tables 1 and 2).

The PP used in this work was obtained from plastic waste containers or as commercially available PP pellets. For simplicity, the commercially available PP pellets are labelled as “pure



PP", and the one from plastic waste containers is referred to as "waste PP". In both cases, for pure PP and waste PP, the FTIR spectra showed the characteristic peaks of C–H bending and stretching at 1375, 1455, and 2837–2950  $\text{cm}^{-1}$  (Fig. S3†), and their fingerprint region was identical, confirming the absence of any organic polymer blend or organic additives in the material from the plastic containers (waste PP).

### 3.1. Polymer solubility and phase diagrams

After the initial screening of solvents based on their HSP and the calculation of the distance  $R_a$ ,  $\alpha$ -pinene and  $\beta$ -limonene were selected for PP and LDPE dissolution considering their solvent–polymer affinity, their bio-based origin, and their wide availability (Table S3 and Fig. S1†). For the pure PP in the  $\alpha$ -pinene system, more than 25 wt% polymer content resulted in a solution too viscous for casting, and more than 30 wt% would not dissolve within three days at 130 °C. Thus, the maximum concentration of pure PP in  $\alpha$ -pinene suitable for membrane fabrication was set to 25 wt%. On the other hand, PP could not be dissolved in  $\beta$ -limonene even after three days at 130 °C at a concentration of 12.5 wt%. In the case of LDPE, the maximum polymer content that could be dissolved at 130 °C in 3 h was 35 wt% for  $\alpha$ -pinene and 40 wt% for  $\beta$ -limonene.

Once fully dissolved at 130 °C, the solution phase separation induced by temperature decrease was investigated by two different methods: (1) cloud point visual observation and (2) calorimetry (DSC). Similar phase separation behavior was observed for the three systems under study: pure PP in

$\alpha$ -pinene, pure LDPE in  $\alpha$ -pinene, and pure LDPE in  $\beta$ -limonene.

The cloud points (CP) or the visualization of the phase separation was possible by optical microscopy, as seen in Fig. 2, 3, S4, and S5.† The appearance of a second phase detected by optical microscopy without polarized light could result from a liquid–liquid (LL) or solid–liquid (SL) phase separation. The solid phase would arise by the crystallization of the polyolefin fraction. The use of polarized light and filters can distinguish the birefringent crystallized phase from amorphous liquid ones and therefore indicate the kind of phase separation (LL or SL). The crystalline phase is characterized by Maltese cross images typically seen in Fig. 2a, 3a, c and S5.†

Crystallization can be detected and quantified by calorimetric methods. DSC was conducted for the PP and LDPE systems with closed liquid panels and led to exact values of the crystallization temperature ( $T_c$ ), which increased as the polymer content increased.<sup>51–54</sup> Fig. 1c and S6† show the crystallization curves for the polyolefin solutions and how the crystallization temperatures shift with the polymer concentration and the type of solvent. In the case of LDPE in  $\alpha$ -pinene, the  $T_c$  ranged from 57.9 °C for 5 wt% polymer content to 72.6 °C for 35 wt%, while in  $\beta$ -limonene the  $T_c$  was 56.1 °C for 5 wt% and 75.4 °C for 40 wt% polymer contents. On the other hand, the  $T_c$  for pure PP in  $\alpha$ -pinene ranged between 45.9 °C and 64.8 °C for 5 wt% and 25 wt%, respectively. In addition, from the DSC curves (Fig. S6†), the peak height and area increased with the increase in polymer content, denoting a larger enthalpy change in the three systems, correlated with the fraction of

**Table 1** Solvent comparison between  $\beta$ -limonene,  $\alpha$ -pinene and other solvents commonly used for polyolefin solubilization

Solvent	Source Bio/fossil	Boiling point °C	Solubility in water $\text{mg L}^{-1}$	Viscosity $\text{mPa s at } 25\text{ °C}$	Vapor pressure $\text{mmHg at } 25\text{ °C}$	Price \$ per kg
$\beta$ -Limonene	Bio	178	13.8	0.846	1.64	10
$\alpha$ -Pinene	Bio	156	2.49	2.100	4.75	3
Benzene	Fossil	80	1–5	0.654	76.00	0.8
Toluene	Fossil	111	526	0.554	28.40	0.8
Chlorobenzene	Fossil	132	0.5	0.806	12.00	0.8
Isooctane	Fossil	99	2.2	0.473	49.30	2
<i>p</i> -Xylene	Fossil	138	165	0.603	8.84	0.5
Trichloroethylene	Fossil	87	1.28	0.545	69.00	0.5

**Table 2** Solvent comparison between  $\alpha$ -pinene and other solvents reported for PP membrane fabrication (PP contents between 5 wt% and 25 wt%) via TIPS

Solvent	Source Bio/fossil	Boiling point °C	Solubility in water $\text{mg L}^{-1}$	Viscosity $\text{mPa s at } 25\text{ °C}$	Vapor pressure $\text{mmHg at } 25\text{ °C}$	Price \$ per kg	CP °C	$T_c$ °C	References
$\alpha$ -Pinene	Bio	156	2.49	2.1	4.75	3	74–88	46–65	This work
Soybean oil	Bio	—	—	60.6	—	0.25	140–150 <sup>a</sup>	~110	Wang <i>et al.</i> <sup>23</sup>
Diphenyl ether	Fossil	258	18	2.6	0.0225	5	137–115	~97	Yave <i>et al.</i> <sup>52</sup>
Diethyl phthalate	Fossil	384	0.022	39	$2.6 \times 10 \times 10^{-6}$	1.5	152–162	~107	Yang <i>et al.</i> <sup>58</sup>
Diamyl phthalate	Fossil	342	0.8	No data available	0.000196	277	193–177	~107	Lin <i>et al.</i> <sup>59</sup>
<i>N,N</i> -Bis(2-hydroxyethyl) tallowamine	Fossil	269	$1 \times 10 \times 10^6$	351.9	$2.8 \times 10 \times 10^{-4}$	0.6	157–147	~104	Lloyd <i>et al.</i> <sup>60</sup>

<sup>a</sup> Solvent mixed with 40 wt% carnauba wax.







**Fig. 2** (a) Polarized and (b) non-polarized optical microscopy cloud point (CP) measurements; (c) crystallization ( $T_c$ ) measurement by DSC temperatures for PP in  $\alpha$ -pinene; and (d) corresponding phase diagram.



**Fig. 3** (a and c) Polarized and (b, d) non-polarized optical microscopy cloud point (CP) measurements; (e) corresponding phase diagram obtained by cloud point and DSC crystallization ( $T_c$ ) measurements for LDPE in  $\alpha$ -pinene and D-limonene.

crystallizable material. The DSC of the waste PP in  $\alpha$ -pinene (Fig. S7†) shows a broader crystallization curve with a peak shifted to higher temperature. This is probably mainly due to their differences in molecular weight and polydispersity (Table S2†).

From the optical microscopy observations and the calorimetric measurements, the phase diagrams depicted in Fig. 1d and 2e were obtained. A gap between curves obtained by the two methods was observed. This could indicate that first, as the temperature decreased, a liquid–liquid phase separation was initiated, with the generation of an amorphous polymer concentrated dispersed phase.<sup>13</sup> As the temperature continued to decrease, the crystallization of the polymer concentrated phase

was initiated as shown in the DSC analysis. As the crystallization proceeds, it can be seen also by the appearance of the birefringent Maltese crosses in the polarized optical microscope.

The crystallization or solid–liquid phase separation follows a nucleation and growth mechanism, which leads to the different final morphologies in the LDPE and PP systems (Fig. 3). In all PP concentrations, spherical structures (spherulites) with diameters around 35  $\mu\text{m}$  were observed at the first stages of the phase separation process.

The phase-separated films prepared from LDPE using both solvents had poor mechanical properties and fell apart upon cooling. This can be related to the observed spherulitic morphology. The grain boundaries are weak points if the entangle-



ment between them is not pronounced, which in this case could be related to the branched structure and low molar mass of LDPE (Table S3†). For this reason, the membrane preparation and performance were focused on the PP in the  $\alpha$ -pinene system only, which led to membranes with higher mechanical stability.

The solubility of polyolefins demonstrated hereby could be useful for coatings, recycling, and any other application requiring a solution process, which typically rely on fossil-based solvents, some of them possessing carcinogenicity or reproductive toxicity.<sup>55–57</sup> Besides the advantage of  $\alpha$ -limonene and  $\alpha$ -pinene of being bio-based and renewable, they are more sustainable options against traditional solvents used for polyolefin solubilization, as shown in Table 1. Their solubility in water is lower than that for toluene and *p*-xylene, and their vapor pressure is lower than those of all other listed solvents, implying a lower exposure to vapors for people working with them. Based on these characteristics, the solvent recovery of the bio-based solvents can be done *via* rotavapor evaporation of the ethanol from the solvent exchange step after the membrane preparation (Fig. S15†).

The viscosity of  $\alpha$ -limonene at room temperature is close to those of the fossil-based solvents, which implies that transporting and handling in a process would not require a large amount of extra energy. However, for industrial scale exploitation of  $\alpha$ -limonene, its price needs to be lower than that as of today.

To better assess the benefits of  $\alpha$ -pinene specifically for PP membrane fabrication, a comparison of  $\alpha$ -pinene with other solvents reported for PP membrane fabrication *via* TIPS is shown in Table 2. As TIPS is driven by a temperature change, the cloud points and crystallization temperatures are of main importance in terms of energy consumption. As can be observed,  $\alpha$ -pinene allows PP membrane formation at lower temperatures, and therefore results in lower energy requirements. Its lower viscosity could be advantageous in terms of processing, and its lower boiling point could facilitate its recovery. It can also be noticed that its price is competitive against other solvents used for PP membrane fabrication. Thus,  $\alpha$ -pinene represents a good alternative for PP membrane fabrication.

### 3.2. Pure PP membrane preparation and characterization

Nine different conditions for pure PP membranes were obtained from varying the polymer content (15 wt%, 20 wt%, or 25 wt%) and the quenching media: air at 20 °C, water at 20 °C, or water at 4 °C.

Passive cooling of the polymer solution on the steel plate by contact with air allowed a slow temperature decrease. By immersing the plate in water, the temperature decreased much faster. The water thermal conductivity is  $0.6 \text{ W m}^{-1} \text{ K}^{-1}$ , while that of air is  $0.025 \text{ W m}^{-1} \text{ K}^{-1}$ , which is 20 times smaller. Cooling is even faster when the water is at 4 °C.

Water and both solvents are practically immiscible. The solubility of  $\alpha$ -pinene and  $\alpha$ -limonene in water is  $2.5 \text{ mg L}^{-1}$  and  $13.8 \text{ mg L}^{-1}$ , and their boiling points are around 157 °C

and 176 °C, respectively. Therefore, there was practically no solvent evaporation, and the solvent–water exchange was negligible. In the subsequent fabrication step, an effective exchange occurred when the film was immersed in ethanol (Fig. 1).

The effect of polymer content and quenching media on the membrane morphology was analyzed using surface and cross-sectional SEM micrographs. The PP membranes prepared with  $\alpha$ -pinene as the solvent featured spherulitic structures with varying size depending on the polymer content and quenching media (Fig. 4). At polymer contents below the critical concentration, phase separation occurs by nucleus formation and growth of a spherical polymer-rich region. After the phase separation, as the spherical nuclei grow, they become interconnected and solidify, forming the membrane structure, and the surrounding polymer-lean space becomes the membrane's pores.<sup>61</sup> This is the case for the PP in the  $\alpha$ -pinene system.

For the membranes quenched in air (Fig. 4a, d, and g), the surface morphology remained similar when varying the PP content, with the spherulite size ranging between approximately 20 and 30  $\mu\text{m}$ , and no visible pores. On the other hand, the use of water at 20 °C as quenching medium limited the spherulite growth (Fig. 4b, e, and h), leading to sizes around 15, 4, and 3  $\mu\text{m}$  for 15, 20, and 25 wt% polymer content, respectively. Lowering the water temperature to 4 °C considerably reduced the spherulite size for all three concentrations (Fig. 4c, f, and i). For 15 wt% polymer content, it reduced to 0.7  $\mu\text{m}$ ; for 20 wt%, to 0.5  $\mu\text{m}$ ; and for 25 wt%, to a size too small to be measured under the given amplification. Such size reduction can be related to the degree of supercooling  $\Delta T$  ( $T_m - T$ ) associated with the use of each quenching medium. According to the polymer crystallization theory, the critical lamella size for crystallization to start is inversely proportional to the supercooling of a polymer solution.<sup>62</sup> This implies that at the lowest temperature of the quenching media (in this case, water at 4 °C), the critical lamella size is smaller, and more nuclei can be formed. Similar conclusions can be made concerning the effect of polymer content. Higher polymer content solutions exhibited a higher  $T_m$  (Fig. S6†), and thus, a larger  $\Delta T$  is applied when quenching compared with lower polymer contents. This also resulted in a larger number of nuclei for higher polymer contents (Fig. 3). These variations in the critical lamella size and the number of nuclei formed led to the observed spherulite size reduction with the increase in polymer content and the decrease in the quenching medium temperature.

The cross-sectional SEM micrographs shown in Fig. 4j–l confirmed that the use of  $\alpha$ -pinene as a solvent resulted in the formation of PP spherulites across the membrane's internal structure. The structure is asymmetric, which can be explained by the different cooling rates of the top and bottom layers. Due to the fabrication method followed in this work, the top of the membranes was directly in contact with the quenching media, while the metallic plate added thermal resistance for the bottom to cool down. This phenomenon has been observed in other PP–solvent systems.<sup>63</sup> The five minutes quenching conditions have a strong influence on the morphology. The







Fig. 4 Surface morphology of pure PP membranes prepared with 15 wt% (a–c), 20 wt% (d–f), and 25 wt% (g–i) PP solutions in  $\alpha$ -pinene and quenched in air at room temperature (a, d and g), water at 20 °C (b, e and h), and water at 4 °C (c, f and i); cross-section images of membranes prepared from 25 wt% PP solutions in  $\alpha$ -pinene quenched under different conditions (j–l).

immersion in water with 20 times higher thermal conductivity rapidly brought the system to the phase separation temperature and promoted fast growth of spherulites. At the time that the film was immersed in ethanol, the membrane formation was practically complete. Films quenched in air demonstrated a denser morphology. We hypothesize that upon immersion in ethanol, the film was not completely solidified yet, and the solvent diffused into the ethanol bath, which resulted in a denser and thinner film.

The results from strain *vs.* stress measurements showed a strong dependency between mechanical properties and the quenching media for the pure PP membranes, while the effect of polymer content was more noticeable on the membrane's toughness (Fig. 5 and Table S4†). Membranes prepared with 15 wt% polymer content and quenched in water at 20 °C had inferior mechanical properties and could not be tested.

Among all tested membranes, Young's modulus and tensile strength were higher for membranes quenched in air at 20 °C (Fig. 5), denoting a larger linear elastic region that can be associated with the denser internal structure observed by SEM. However, the same membranes had lower fracture strain and

toughness. In these two aspects, membranes quenched in water at 4 °C had higher values. This can be associated with the dense structure of the membranes quenched in air.

Compared to other PP membranes reported in the literature with spongelike or cellular structures, the membranes obtained in this work had lower mechanical properties.<sup>23,64</sup> Thus, it can be assumed that the PP membrane spherulitic morphology significantly affects their mechanical properties. A similar conclusion was reported for membranes prepared with poly(vinylidene fluoride) (PVDF), another aliphatic semicrystalline polymer.<sup>65</sup> In their study, the same material had very different mechanical properties depending on the final morphology of the membrane, the highest for interconnected cellular structures and the lowest for interconnected globules. Thus, the same situation could occur for the PP membranes obtained in this work.

Slight differences in the melting and crystallization temperatures were observed after the film preparation using different quenching conditions (Fig. S8†). The  $T_m$  decreased from 167 °C to 162 °C, while the  $T_c$  remained close to the original value of 118 °C except for the membrane quenched in water at 20 °C,





Fig. 5 Mechanical properties of pure PP membranes prepared with 15, 20, and 25 wt% polymer contents in  $\alpha$ -pinene and quenched in air at room temperature, water at 20 °C, and water at 4 °C. (a) Young's modulus, (b) toughness, (c) tensile strength and (d) fracture strain.

which increased to 119 °C. The crystallization and melting enthalpies of the prepared membranes varied less than 5% compared to the pure original polymer pellets, denoting a similar degree of crystallinity. Similar results were obtained with all polymer contents (Fig. S8 and Tables S5, S6†).

### 3.3. PP membrane performance

We report for the first time  $\alpha$ -pinene and D-limonene as greener solvents for PP and LDPE dissolution and membrane preparation. We explored and demonstrated here the potential application for membrane technology, focusing on oil–water emulsion separation, which is relevant for applications such as produced water removal or oil spill clean-up.<sup>66–68</sup>

All prepared films were highly hydrophobic, with water contact angles of approximately 100° (Fig. S10†), as expected for PP films.<sup>68,69</sup> Films quenched in water at 20 °C were the most hydrophobic. Surface roughness can increase the water contact angle by inducing a Cassie state,<sup>70</sup> which might contribute to the higher values for those films due to their rougher surfaces. The membranes prepared from 20 and 25 wt% pure PP solutions exhibited under-oil (in hexane, heptane, and toluene) water contact angles above 150° (Fig. S11†), classifying them as under-oil superhydrophobic and indicating their suitability for water-in-oil emulsion separation.

Based on the selection of pure PP membranes, similar conditions were applied to fabricate membranes from PP plastic waste as the polymer source. The dope solution of waste PP had a lower viscosity than that of commercial pure PP solution.

This difference can be attributed to its lower molecular weight (Table S2†), which also lowered the mechanical properties of the final waste PP membranes compared with the ones prepared from pure PP pellets under the same conditions (Table S4†). Thus, higher waste PP polymer content was able to be dissolved at the same temperature as pure PP (130 °C), resulting in mechanically stable membranes that were successfully tested for the separation process. Waste PP concentrations that allowed membrane formation were between 25 and 30 wt%. Quenching in water at 4 °C led to membranes with the best mechanical stability up to 18 MPa for 30 wt% waste PP (Fig. S12c and d†). SEM images revealed a surface and cross-section spherulitic morphology like those of pure PP membranes, with an asymmetric structure (Fig. S13†), and similar under-oil water contact angles above 150° (Fig. S12†).

The thermal properties of the waste PP membranes were compared with those of the membranes prepared from commercial PP pellets (Fig. S14†). The TGA curves showed that 90% of the waste PP membrane weight is lost at around 350 °C, lower than the 376 °C observed for pure PP. In the case of melting and crystallization behavior, the DSC curves showed a lower  $T_m$  of 161 °C and a higher  $T_c$  of 123 °C compared to the pure PP pellets ( $T_m$  of 167 °C and  $T_c$  of 118 °C).

After an initial heptane filtration test performed with mechanically stable membranes (Table 3), six fabrication conditions for PP membranes were chosen for further testing. Filtration tests of selected membranes were performed for *n*-heptane, *n*-hexane, and toluene (Fig. 6). The permeance was lower for higher polymer content and decreased with the



hydrocarbon viscosity. In the case of pure PP membranes, lower permeance was observed for membranes with higher polymer content, which can be associated with smaller pore size, as observed by SEM. The permeance was the highest for *n*-hexane, the hydrocarbon with the lowest viscosity (Table S1†), ranging from 0.28 to 0.7 L m<sup>-2</sup> h<sup>-1</sup> bar<sup>-1</sup>, followed by heptane and toluene with 0.25 to 0.56 and 0.22 to 0.48 L m<sup>-2</sup> h<sup>-1</sup> bar<sup>-1</sup>, respectively.

The permeance of membranes prepared from waste PP membranes was practically independent of the dope solution polymer content, since the upper layer morphologies of the membranes prepared from 25 and 30 wt% were similar (Fig. S13†).

All membranes demonstrated a good separation performance for water-in-toluene emulsions (Fig. 6). The two best performing pure PP membranes (22.5 wt% PP quenched in water at 20 °C and 25 wt% when quenched at 20 °C) demonstrated 95.7% water rejection, while both tested waste PP membranes had rejections of 95.0% and 94.9%. These results imply around 99.97% toluene purity in terms of water content. All obtained permeance, water rejection, and water content in the permeate values are shown in Table S7.† From DLS measurements, it was observed that the water drops in the emulsion had diameters above 200 nm.

**Table 3** PP membranes initially tested for pure hydrocarbon filtration

Sample	PP source	Polymer content (wt%)	Quenching media	Heptane permeance (L m <sup>-2</sup> h <sup>-1</sup> bar <sup>-1</sup> )
20%_4 °C	Pure	20	Water at 4 °C	0.69
22.5%_4 °C	Pure	22.5	Water at 4 °C	0.44
25%_4 °C	Pure	25	Water at 4 °C	0.00
22.5%_20 °C	Pure	22.5	Water at 20 °C	0.61
25%_20 °C	Pure	25	Water at 20 °C	0.28
W25%_4 °C	Waste	25	Water at 4 °C	0.30
W27.5%_4 °C	Waste	27.5	Water at 4 °C	0.32
W30%_4 °C	Waste	30	Water at 4 °C	0.06

Comparable toluene purity values have been reported by other hydrophobic membranes.<sup>50,68,69,71</sup> Tao *et al.*<sup>50</sup> reported a toluene purity of 99.96% after the filtration of a water-in-toluene emulsion with 1% water content utilizing a modified PVDF membrane. Kansara *et al.*<sup>69</sup> prepared superhydrophobic membranes by coating alkylsiloxane-silica nanoparticles on a PP fabric and obtained a toluene purity above 99% from a 10% water containing water-in-toluene emulsion.

The use of renewable bio-based solvents and plastic waste reported in this work represents a greener and more straightforward method to fabricate PP membranes for water-in-oil emulsion separation.

## 4. Conclusions

Bio-based solvents were successfully employed for PP and LDPE dissolution. LDPE was dissolved in  $\alpha$ -pinene and  $\beta$ -limonene with an upper solubility limit of 35 wt% and 40 wt% polymer content at 130 °C, while PP was soluble in  $\alpha$ -pinene with up to 25 wt% polymer content. The phase diagram was evaluated for three systems indicating a liquid-liquid phase separation and a further crystallization of the polymer concentrated phase with a spherulitic morphology at temperatures below 100 °C. PP membranes were successfully prepared with  $\alpha$ -pinene as solvent *via* TIPS utilizing commercial and waste polymers, where the membrane morphology and separation performance strongly depended on the quenching media and polymer content. Water as quenching medium resulted in smaller spherulite and pore sizes and better mechanical properties, whereas quenching in air led to a denser membrane structure. Polymer contents with between 20 and 25 wt% of pure PP and between 30 and 35 wt% of waste PP led to stable self-standing membranes. Water-in-toluene emulsion separation performance with 95% water rejection and a toluene purity of approximately 99.97% were achieved. This study broadens the alternatives for polyolefin



**Fig. 6** Pure and waste PP membrane performance: (a) hydrocarbon permeance and (b) water rejection in the separation of water in toluene emulsion.





(PP and LDPE) dissolution and membrane fabrication with renewable non-toxic bio-based solvents while revalorizing plastic waste, which can be of benefit for the polymers and membrane fields in the transition to a circular economy following the green chemistry principles.

## Author contributions

Malinalli Ramírez-Martínez: methodology, investigation, validation, visualization, formal analysis, and writing—original draft. Sandra L. Aristizábal: conceptualization, supervision, and writing—review & editing. Gyorgy Szekely: supervision, writing—review & editing. Suzana P. Nunes: conceptualization, methodology, resources, funding acquisition, project administration, supervision, and writing—review & editing.

## Conflicts of interest

There are no conflicts to declare.

## Acknowledgements

This work was sponsored by the King Abdullah University of Science and Technology (KAUST). The authors acknowledge Dr Jiayi Zhao and Prof. Sanjay Rastogi for their support in optical microscopy observations.

## References

- 1 D. S. Sholl and R. P. Lively, *Nature*, 2016, **532**, 435–437.
- 2 S. P. Nunes and K.-V. Peinemann, *Membrane Technology in the Chemistry Industry*, Wiley-VCH, 2nd edn, 2006.
- 3 R. W. Baker, *Membrane Technology and Applications*, California, 2004.
- 4 H. Lin and Y. Ding, *J. Polym. Sci.*, 2020, **58**, 2433–2434.
- 5 S. Chisca, V.-E. Musteata, W. Zhang, S. Vasylevskyi, G. Falca, E. Abou-Hamad, A.-H. Emwas, M. Altunkaya and S. P. Nunes, *Science*, 2022, **376**, 1105–1110.
- 6 W. Xie, T. Li, A. Tiraferri, E. Drioli, A. Figoli, J. C. Crittenden and B. Liu, *ACS Sustainable Chem. Eng.*, 2021, **9**, 50–75.
- 7 S. P. Nunes, P. Z. Culfaz-Emecen, G. Z. Ramon, T. Visser, G. H. Koops, W. Jin and M. Ulbricht, *J. Membr. Sci.*, 2020, **598**, 117761–117761.
- 8 P. Yadav, N. Ismail, M. Essalhi, M. Tysklind, D. Athanassiadis and N. Tavajohi, *J. Membr. Sci.*, 2021, **622**, 118987–118987.
- 9 X. Dong, D. Lu, T. A. Harris and I. C. Escobar, *Membranes*, 2021, **11**, 309.
- 10 M. Liu, S. Liu, Z. Xu, Y. Wei and H. Yang, *Front. Chem. Sci. Eng.*, 2016, **10**, 57–75.
- 11 D.-M. Wang and J.-Y. Lai, *Curr. Opin. Chem. Eng.*, 2013, **2**, 229–237.
- 12 A. K. Holda and I. F. J. Vankelecom, *J. Appl. Polym. Sci.*, 2015, **132**, 42130.
- 13 J. F. Kim, J. H. Kim, Y. M. Lee and E. Drioli, *AIChE J.*, 2015, **62**, 461–490.
- 14 S. Jiang and B. P. Ladewig, *Curr. Opin. Green Sustain. Chem.*, 2020, **21**, 1–8.
- 15 H. H. Wang, J. T. Jung, J. F. Kim, S. Kim, E. Drioli and Y. M. Lee, *J. Membr. Sci.*, 2019, **574**, 44–54.
- 16 D. Kim and S. P. Nunes, *Green Sustainable Chem.*, 2021, **28**, 100427–100427.
- 17 A. Figoli, T. Marino, S. Simone, E. Di Nicolò, X.-M. Li, T. He, S. Tornaghi and E. Drioli, *Green Chem.*, 2014, **16**, 4034–4059.
- 18 D. Zou, S. P. Nunes, I. F. Vankelecom, A. Figoli and Y. M. Lee, *Green Chem.*, 2021, **23**, 9815–9843.
- 19 G. Szekely, M. F. Jimenez-Solomon, P. Marchetti, J. F. Kim and A. G. Livingston, *Green Chem.*, 2014, **16**, 4440–4473.
- 20 T. Marino, F. Galiano, A. Molino and A. Figoli, *J. Membr. Sci.*, 2019, **580**, 224–234.
- 21 M. A. Rasool, C. Van Goethem and I. F. J. Vankelecom, *Sep. Purif. Technol.*, 2020, **232**, 115903–115903.
- 22 Y. Medina-Gonzalez, P. Aimar, J. F. Lahitte and J. C. Remigy, *Int. J. Sustainable Eng.*, 2011, **4**, 75–83.
- 23 Y. J. Wang, Z. P. Zhao, Z. Y. Xi and S. Y. Yan, *J. Membr. Sci.*, 2018, **548**, 332–344.
- 24 M. A. Rasool and I. F. Vankelecom, *J. Membr. Sci.*, 2021, **618**, 118674.
- 25 M. A. Rasool and I. F. Vankelecom, *Membranes*, 2021, **11**, 418.
- 26 J. Cavalcante, R. Hardian and G. Szekely, *Sustainable Mater. Technol.*, 2022, e00448.
- 27 X. Dong, T. J. Jeong, E. Kline, L. Banks, E. Grulke, T. Harris and I. C. Escobar, *J. Membr. Sci.*, 2020, **614**, 118510.
- 28 N. Ismail, M. Essalhi, M. Rahmati, Z. Cui, M. Khayet and N. Tavajohi, *Green Chem.*, 2021, **23**, 2130–2147.
- 29 Market volume of polypropylene worldwide from 2015 to 2021, with a forecast for 2022 to 2029 (in million metric tons), <https://www.statista.com/statistics/1245169/polypropylene-market-volume-worldwide/>, (accessed June 29, 2022).
- 30 Market volume of polyethylene worldwide from 2015 to 2021, with a forecast for 2022 to 2029 (in million metric tons), <https://www.statista.com/statistics/1245162/polyethylene-market-volume-worldwide/>, (accessed June 29, 2022).
- 31 J. M. Garcia and M. L. Robertson, *Science*, 2017, **358**, 870–872.
- 32 Plastics – the facts 2020, [https://plasticseurope.org/wp-content/uploads/2021/09/Plastics\\_the\\_facts-WEB-2020\\_versionJun21\\_final.pdf](https://plasticseurope.org/wp-content/uploads/2021/09/Plastics_the_facts-WEB-2020_versionJun21_final.pdf), (accessed May 23, 2022).
- 33 The new plastics economy: Rethinking the future of plastics & catalysing action, <https://emf.thirdlight.com/link/cap0qk3wwwk0-l3727v/@/preview/2>, (accessed June 10, 2022).
- 34 P. S. Goh, M. H. D. Othman and T. Matsuura, *Membranes*, 2021, **11**, 782.
- 35 M. Al-Shaeli, R. A. Al-Juboori, S. Al Aani, B. P. Ladewig and N. Hilal, *Sci. Total Environ.*, 2022, 156014.



- 36 B. A. Pulido, O. S. Habboub, S. L. Aristizabal, G. Szekely and S. P. Nunes, *ACS Appl. Polym. Mater.*, 2019, **1**, 2379–2387.
- 37 W.-h. Lai, C.-y. Hong, H.-h. Tseng and M.-y. Wey, *Environ. Res.*, 2021, **195**, 110760–110760.
- 38 M. K. Keleş and Y. Uysal, *Clean Technol. Environ. Policy*, 2021, **23**, 1431–1442.
- 39 J. Gershenzon and N. Dudareva, *Nat. Chem. Biol.*, 2007, **3**, 408–414.
- 40 A. Pereira, M. Fraga-Corral, P. García-Oliveira, C. Jimenez-Lopez, C. Lourenço-Lopes, M. Carpena, P. Otero, P. Gullón, M. Prieto and J. Simal-Gandara, *Food Funct.*, 2020, **11**, 8493–8515.
- 41 W. Schwab, C. Fuchs and F. C. Huang, *Eur. J. Lipid Sci. Technol.*, 2013, **115**, 3–8.
- 42 S. Kandi, V. Godishala, P. Rao and K. V. Ramana, *Biomed. Biotechnol.*, 2015, **3**, 8–10.
- 43 E. Yara-Varón, A. Selka, A.-S. Fabiano-Tixier, M. Balcells, R. Canela-Garayoa, A. Bily, M. Touaibia and F. Chemat, *Green Chem.*, 2016, **18**, 6596–6608.
- 44 C. D. Tanzi, M. A. Vian, C. Ginies, M. Elmaataoui and F. Chemat, *Molecules*, 2012, **17**, 8196–8205.
- 45 M. M. Cascant, C. Breil, S. Garrigues, M. de la Guardia, A. S. Fabiano-Tixier and F. Chemat, *Anal. Bioanal. Chem.*, 2017, **409**, 3527–3539.
- 46 G. Papa, J. Kirby, N. M. Konda, K. Tran, S. Singh, J. D. Keasling, G. F. Peter and B. A. Simmons, *Green Chem.*, 2017, **19**, 1117–1127.
- 47 I. John, K. Muthukumar and A. Arunagiri, *Int. J. Green Energy*, 2017, **14**, 599–612.
- 48 C. M. Hansen, *Hansen solubility parameters: A user's handbook*, 2nd edn, 2007.
- 49 D. W. Van Krevelen and K. Te Nijenhuis, *Properties of polymers: their correlation with chemical structure; their numerical estimation and prediction from additive group contributions*, Elsevier, 2009.
- 50 M. Tao, L. Xue, F. Liu and L. Jiang, *Adv. Mater.*, 2014, **26**, 2943–2948.
- 51 D. R. Lloyd, K. E. Kinzer and H. S. Tseng, *J. Membr. Sci.*, 1990, **52**, 239–261.
- 52 W. Yave, R. Quijada, D. Serafini and D. R. Lloyd, *J. Membr. Sci.*, 2005, **263**, 146–153.
- 53 H. Matsuyama, M. Teramoto, S. Kudari and Y. Kitamura, *J. Appl. Polym. Sci.*, 2001, **82**, 169–177.
- 54 H. Matsuyama, T. Maki, M. Teramoto and K. Asano, *J. Membr. Sci.*, 2002, **204**, 323–328.
- 55 S. L. Wong, N. Ngadi and T. A. T. Abdullah, *Appl. Mech. Mater.*, 2014, **695**, 170–173.
- 56 A. J. Hadi, G. F. Najmuldeen and I. Ahmed, *J. Polym. Eng.*, 2012, **32**, 585–591.
- 57 D. S. Achilias, C. Roupakias, P. Megalokonomos, A. A. Lappas and V. Antonakou, *J. Hazard. Mater.*, 2007, **149**, 536–542.
- 58 Z. Yang, P. Li, L. Xie, Z. Wang and S. C. Wang, *Desalination*, 2006, **192**, 168–181.
- 59 Y. K. Lin, G. Chen, J. Yang and X. L. Wang, *Desalination*, 2009, **236**, 8–15.
- 60 D. R. Lloyd, S. S. Kim and K. E. Kinzer, *J. Membr. Sci.*, 1991, **64**, 1–11.
- 61 K. Kamide, H. Iijima and S. Matsuda, *Polym. J.*, 1993, **25**, 1113–1131.
- 62 H. G. Elias, in *Macromolecules, Volume 3: Physical Structures and Properties*, 2008, pp. 191–238.
- 63 H. Matsuyama, M. Yuasa, Y. Kitamura, M. Teramoto and D. R. Lloyd, *J. Membr. Sci.*, 2000, **179**, 91–100.
- 64 W. Yave, R. Quijada, M. Ulbricht and R. Benavente, *Polymer*, 2005, **46**, 11582–11590.
- 65 P. Sukitpaneenit and T.-S. Chung, in *Hollow Fiber Membranes*, Elsevier, 2021, pp. 333–360.
- 66 B. Doshi, M. Sillanpää and S. Kalliola, *Water Res.*, 2018, **135**, 262–277.
- 67 K. Gaaseidnes and J. Turbeville, *Pure Appl. Chem.*, 1999, **71**, 95–101.
- 68 Y. Sun, Z. Yang, L. Li, Z. Wang and Q. Sun, *J. Membr. Sci.*, 2019, **581**, 224–235.
- 69 A. M. Kansara, S. G. Chaudhri and P. S. Singh, *RSC Adv.*, 2016, **6**, 61129–61136.
- 70 P. Roach, N. Shirtcliffe and M. Newton, *Soft Matter*, 2008, **4**, 224–240.
- 71 X. Zhang, C. Liu, J. Yang, X. J. Huang and Z. K. Xu, *J. Membr. Sci.*, 2021, **624**, 118976–118976.

